Disorder-Induced Topological State Transition in the Optical Skyrmion Family

Changxu Liu*
Department of Mathematics, Physics and Electrical Engineering, Northumbria University, Newcastle Upon Tyne NE1 8ST, United Kingdom
and Chair in Hybrid Nanosystems, Nanoinstitute Munich, Faculty of Physics, Ludwig-Maximilians-Universitaet Muenchen, 80539 Muenchen, Germany

Shuang Zhang
Department of Physics, University of Hong Kong, Hong Kong, China
and Department of Electrical Engineering, University of Hong Kong, Hong Kong, China

Stefan A. Maier
School of Physics and Astronomy, Monash University, Clayton, Victoria 3800, Australia;
Chair in Hybrid Nanosystems, Nanoinstitute Munich, Faculty of Physics, Ludwig-Maximilians-Universitaet Muenchen, 80539 Muenchen, Germany;
and Department of Physics, Imperial College London, London SW7 2AZ, United Kingdom

Haoran Ren†
School of Physics and Astronomy, Monash University, Clayton, Victoria 3800, Australia

(Received 8 June 2022; accepted 7 December 2022; published 23 December 2022)

Skyrmions endowed with topological protection have been extensively investigated in various platforms including magnetics, ferroelectrics, and liquid crystals, stimulating applications such as memories, logic devices, and neuromorphic computing. While the optical counterpart has been proposed and realized recently, the study of optical skyrmions is still in its infancy. Among the unexplored questions, the investigation of the topology induced robustness against disorder is of substantial importance on both fundamental and practical sides but remains elusive. In this Letter, we manage to generate optical skyrmions numerically in real space with different topological features at will, providing a unique platform to investigate the robustness of various optical skyrmions. A disorder-induced topological state transition is observed for the first time in a family of optical skyrmions composed of six classes with different skyrmion numbers. Intriguingly, the optical skyrmions produced from a vectorial hologram are exceptionally robust against scattering from a random medium, shedding light on topological photonic devices for the generation and manipulation of robust states for applications including imaging and communication.

DOI: 10.1103/PhysRevLett.129.267401

Introduction.—Skyrmions, originally proposed by Skyrme in the 1960s to describe the stability of the constituents of elementary particles [1], are vortexlike formations of a field that cannot be eliminated by any smooth transformation. After first realizations in magnetic systems [2–6], the topology-protected quasiparticles have been achieved in fundamentally different classical and quantum platforms, ranging from liquid crystals [7–10], ferroelectrics [11–14] to polariton superfluids [15] and acoustics [16].

Recently, the photonic counterpart of skyrmions has been first realized in surface plasmon polaritons [17], utilizing the evanescent electric field to form the desired topology. Later, optical skyrmions were achieved in a repertoire of systems based on different vector fields, including electric [18] or magnetic [19,20] fields in real space and photonic spin or Stokes vectors in artificial space [21–28]. In analogy with Dzyaloshinskii Moriya interaction in magnetic skyrmion [2–6], various types of light mater interactions, including spin-orbit coupling [21–23], photonic quantum spin Hall effect [25], and artificial photonic gauge field [24], were utilized to form vectorial fields matching the topology of a specific class of skyrmions. Meanwhile, optical skyrmions free from interaction with materials can be achieved in free space through the superposition of structured light [20,26–29]. Néel and Bloch-type optical skyrmions have been proposed in the polarization fields [29]. Optical skyrmions with different topologies have been realized from a digital hologram system based on Stokes vector fields in the artificial space [27], providing flexibility not achieved by the magnetic counterpart.

In magnetic systems, the nontrivial topology endows skyrmion with unparalleled robustness to perturbation,

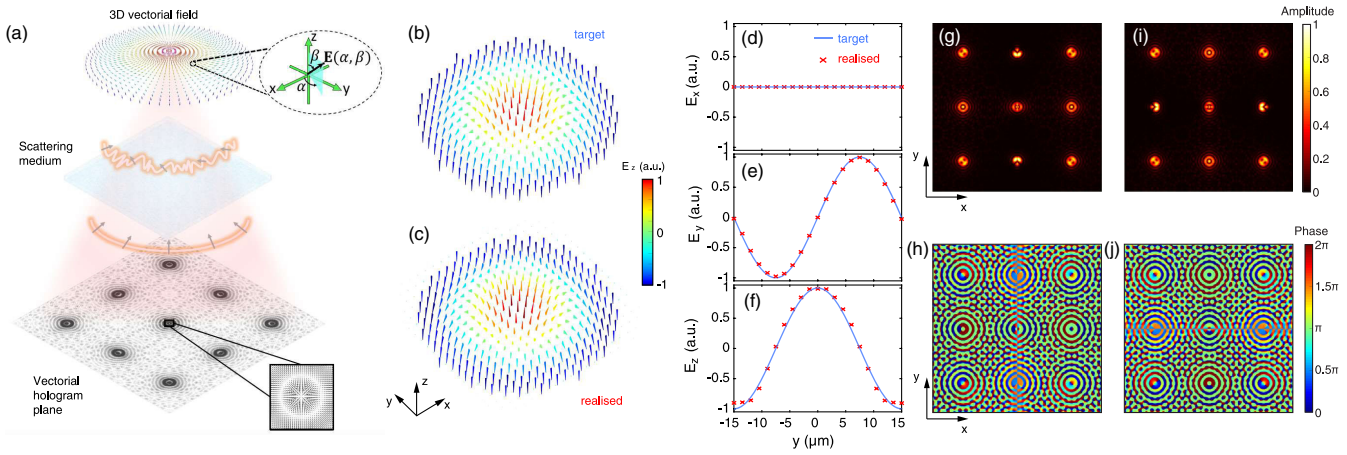

FIG. 1. Realization of the Néel-type skyrmion. (a) Artistic view of a vectorial hologram for creating an optical skyrmion that is digitized by 3D vectorial fields in real space. Fluctuations in amplitude and phase can be introduced from the scattering medium. (b) An ideal Néel-type skyrmion ($N_{\mathrm{sk}} = 1$, $\nu = 1$, $h = 0$). (c) The realized quasiparticle composed of vectorial electric field. (d)–(f) A comparison of the electric field in the symmetric axis. (g)–(j) The designed amplitude and phase on the hologram plane, i.e., the bottom plane shown in (a). The amplitude and phase polarized along the x direction are shown in (g) and (h), while the amplitude and phase polarized along the y direction are shown in (i) and (j).

suggesting a platform for various applications such as memory, logic devices, and neuromorphic computing [4,30,31]. While the robustness of magnetic skyrmions has been extensively studied [32–45], a systematic investigation of optical skyrmions with the presence of disorder remains elusive. A comprehensive understanding of robustness is indispensable for the further progress of optical skyrmions, aiming at practical applications including imaging, microscopy, communication, and encryption [46].

Inspired by recent advances in the manipulation of three-dimensional (3D) vectorial fields [47–52], we propose a novel platform for the realization of arbitrary optical skyrmions in real space. Quasiparticles with different skyrmion numbers [53] ($N_{\mathrm{sk}} = 1, -1, \frac{1}{2}, \frac{1}{4}$) are achieved numerically based on the electric field vectors from a vectorial hologram. More importantly, we provide a comprehensive investigation of the robustness against disorder, accounting for the imperfection of hologram devices or light propagation in a scattering medium. To the best of our knowledge, we report here the first disorder-induced state transition in optical skyrmions. The state transition is confirmed as a general phenomenon for a family of quasiparticles, ranging from anti-skyrmions, skyrmions, to half- and quarter- skyrmions. Surprisingly, the unique topology of skyrmion endows the optical quasi-particle with an unprecedented robustness against disorder in phase, maintaining the nontrivial feature under fluctuations up to 0.7π. Our Letter not only contributes to the fundamental physics by offering the first comparison of the disorder-induced state transition for the skyrmion family, but also sheds light on practical applications such as imaging and communications for optical skyrmions where the random scattering is inevitable.

Results.—The physical mechanism of using a vectorial hologram for creating arbitrary optical skyrmions is illustrated in Fig. 1(a). Based on the principle of 3D vectorial holography [48], these 3D vectorial fields at given positions in the image plane can be physically determined from a 2D vector field distribution in the hologram plane. A 3D vectorial field is represented by $E(\alpha, \beta)$ in a spherical coordinate system, where α and β are the azimuthal and polar angles, respectively [inset of Fig. 1(a)]. We use the generalized vectorial diffraction theory to evaluate the orthogonal electric field components (E_x, E_y, E_z) of a 3D vectorial field under the tight focusing condition, which can independently correlate the orthogonal electric field components of the 3D vectorial field $E(\alpha, \beta)$ with different azimuthal and radial components of a 2D vector field in the hologram plane. More details can be found in the Supplemental Material [54].

Utilising the vectorial hologram, we are able to achieve a 3D electric field texture point by point on the 2D image plane, and produce the desired configuration matching the topology of optical skyrmions. The topological property of a 2D quasiparticle is characterized by the skyrmion number defined as

$$N_{\mathrm{sk}} = \frac{1}{4\pi} \iint_S \mathbf{n} \cdot \left(\frac{\partial \mathbf{n}}{\partial x} \times \frac{\partial \mathbf{n}}{\partial y} \right) \mathrm{d}x\mathrm{d}y \qquad (1)$$

with the vector field $\mathbf{n}$ forming a quasiparticle constrained in a 2D region S. A nontrivial skyrmion number counts the number of winding for vectors going from centre to boundary. Accompanying the skyrmion number, the vorticity number (ν) and the helicity number (h) are introduced for a complete characterization of a skyrmion [53]. Three

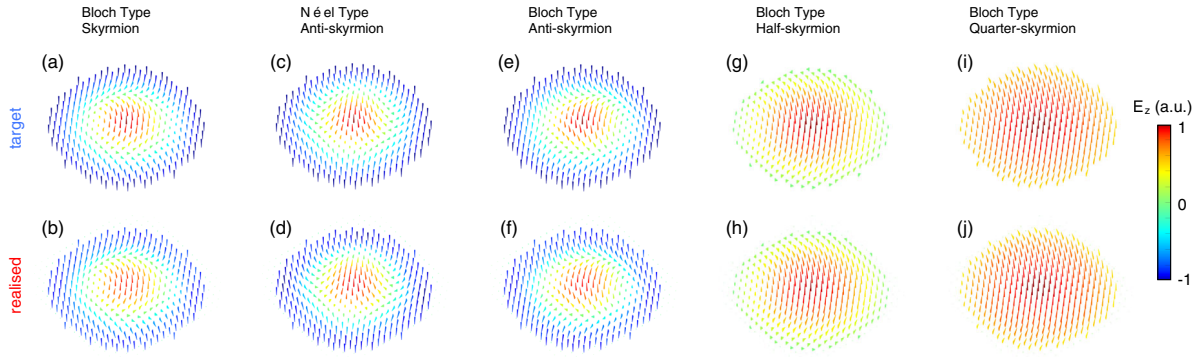

FIG. 2. Realization of different classes of optical skyrmions based on vectorial hologram. The first row demonstrates the ideal textures and the second row shows the realized quasiparticles composed of vectorial electric fields. Five classes are included: (a)–(b) Bloch-type skyrmion ($N_{\mathrm{sk}} = 1$, $\nu = 1$, and $h = (\pi/2)$); (c)–(d) Néel-type anti-skyrmion ($N_{\mathrm{sk}} = 1$, $\nu = -1$, and $h = 0$); (e)–(f) Bloch-type anti-skyrmion ($N_{\mathrm{sk}} = 1$, $\nu = -1$, and $h = (\pi/2)$); (g)–(h) Bloch-type half-skyrmion ($N_{\mathrm{sk}} = \frac{1}{2}$, $\nu = 1$, and $h = (\pi/2)$); (i)–(j) Bloch-type quarter-skyrmion ($N_{\mathrm{sk}} = \frac{1}{4}$, $\nu = 1$, and $h = (\pi/2)$).

distinct values of $(N_{\mathrm{sk}}, \nu, h)$ differentiate a particular class of quasiparticle from the skyrmion family. More details can be found in the Supplemental Material [54].

Figures 1(b)–1(j) summarize the realization of a Néel-type skyrmion based on the proposed vectorial hologram. An ideal Néel-type skyrmion is illustrated in Fig. 1(b). The arrow represents the electric field, and its color measures the magnitude of E_z. The quasiparticle has an axisymmetric texture, with the electric field vector rotating radially from downwards to upwards pointing. Figure 1(c) shows the 3D electric field realized. Discrete points from the skyrmion are selected and produced through the vectorial hologram. The accuracy is confirmed by a comparison between the textures in Figs. 1(b) and 1(c) with a negligible difference. We further provide a quantitative comparison in Figs. 1(d) to 1(f), where the electric fields in three orthogonal directions are shown, respectively. The field distribution along the symmetric axis y is selected, with solid blue lines for an ideal skyrmion and red crosses for the realized one. The zero helicity induces no field along x, while both E_y and E_z follow a sinusoidal-shaped curve. Despite differences between the target and realization, the topological feature is well reproduced. The skyrmion number N_{sk} is numerically calculated based on Eq. (1), with region S defined as the circle with radius of 15 μm. The value of the realized Néel-type skyrmion is 0.98, close to the ideal value of 1. To realize the field texture shown in Fig. 1(c), we utilize a vectorial hologram along both x and y polarizations. The designed amplitude and phase are demonstrated in Fig. 1(g)–1(j).

To demonstrate the versatility of the proposed method, we realized another five classes of skyrmions with distinct textures. Figure 2(a) shows a skyrmion of Bloch-type with a nonzero helicity $h = (\pi/2)$. Compared with Néel-type with the same values of N_{sk} and ν [Fig. 1(a)], it has a chiral feature in the x-y plane. Meanwhile, antiskyrmions, quasiparticles with the opposite sign of N_{sk}, are shown in Figs. 2(c) and 2(e). Compared to their counterparts [Figs. 1(b) and 2(a)], the sign of the vorticity number is reversed from 1 to -1, while the value of h decides whether it is a Néel or Bloch type. In addition to quasiparticles with integer topological numbers, we further choose two classes of textures with fractional skyrmion numbers; the half-skyrmion (or merons) with $N_{\mathrm{sk}} = \frac{1}{2}$ and the quarter-skyrmion with $N_{\mathrm{sk}} = \frac{1}{4}$. The vector field only rotates a portion of a complete swap from downwards to upwards when approaching the centre [Figs. 2(g) and 2(i)]. More details can be found in the Supplemental Material [54]. All realized electric field textures (second row of Fig. 2) replicate the desired topology (first row of Fig. 2). The perfect match is confirmed quantitatively by the calculated (ideal) skyrmion numbers; 0.99(1) for Bloch-type skyrmion, $-0.98(-1)$ for Néel-type anti-skyrmion, $-0.99(-1)$ for Bloch-type anti-skyrmion, 0.504(0.5) for Bloch-type half-skyrmion, and 0.247(0.25) for Bloch-type quarter-skyrmion. The calculated phase and amplitude in the hologram plane for all five classes can be found in the Supplemental Material [54].

With the flexibility to produce a family of skyrmions, we implement a comprehensive investigation to elucidate how disorder can impair topological-protected quasiparticles. We introduce two types of disorder in our vectorial hologram: the fluctuations in phase and amplitude. Correspondingly, the amplitude $A(x, y)$ and phase $P(x, y)$ on the hologram plane (x, y) can be modeled as

$$\begin{aligned} A(x, y) &= A_0(x, y) + \delta_A U_1(x, y), \\ P(x, y) &= P_0(x, y) + \delta_P U_2(x, y), \end{aligned} \tag{2}$$

with $A_0(x, y)$ and $P_0(x, y)$ the computed amplitude and phase, $U_{1,2}(x, y)$ independent uniform distributions within $[-1, 1]$. The value of δ_A (δ_P) represents a random fluctuation in the amplitude (phase), serving as a measurement

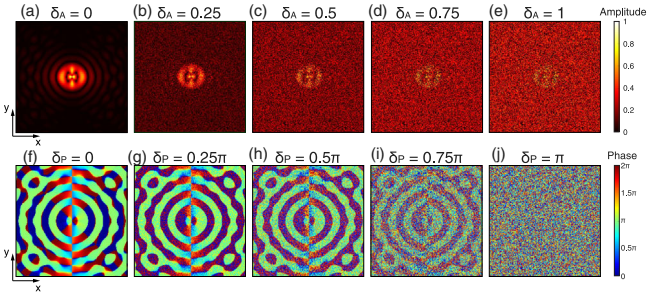

FIG. 3. A demonstration of disorder introduced in amplitude (a)–(e) and phase (f)–(j) on the hologram plane. The amplitude and phase are selected from the central region in Figs. 1(g) and 1(h).

of the strength of the disorder. Figure 3 shows the amplitude and phase distributions with various levels of disorder. Figures 3(a)–3(e) illustrate the distributions of amplitude with different values of δ_A, while Figs. 3(f)–3(j) show the distributions of phase. The original amplitude [Fig. 3(a)] and phase [Fig. 3(f)] are chosen from the central part of Fig. 1(f) and 1(g), respectively. For both amplitude and phase, the increment of the fluctuation obscures the well-defined pattern and consequently impairs the skyrmions on the image plane.

Figure 4 summarizes the robustness of a Néel-type skyrmion against fluctuations, demonstrating the disorder-induced state transition. To make a quantitative analysis, we calculate the skyrmion number N_{sk} of the electric vectorial field texture formed on the image plane. Figure 4(a) shows the situation with the fluctuation only in phase. When δ_P increases from 0 to π, the skyrmion number experiences a prominent degradation from 1 to 0. The value of 1 represents an ideal skyrmion, while zero refers to a fully randomized pattern. Interestingly, we observe strong robustness against phase disorder. The N_{sk} maintains its original value when $\delta_P < 0.7\pi$, decreasing from 0.98 to 0.92. Further increment of disorder in phase induces a sharp degradation. The four insets in Fig. 4(a) are the electric field distributions under different values of δ_P, demonstrating the state transition from a Néel-type skyrmion to a fully-randomized pattern.

The evolution of the skyrmion with the disorder in amplitude is shown in Fig. 4(b) with $\delta_P = 0$. Again, we observe a disorder-induced state. However, the skyrmion is vulnerable to the disorder in amplitude. Similarly, we demonstrate the electric field distributions as the insets in Fig. 4(b). The amplitude fluctuation has an intense impact on the edge of the skyrmion. Large δ_A randomizes the electric field on the edge and results in the degradation of N_{sk}.

We further investigate the case when both the fluctuation in phase and amplitude exist, with the results summarized in Figs. 4(c)–4(d). Figure 4(c) shows the evolution of N_{sk} as the increment of the two different types of disorder. The color in the (δ_P, δ_A) plane represents the value of

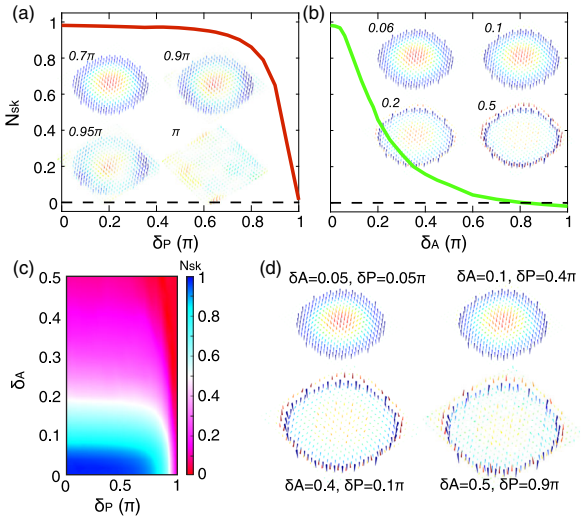

FIG. 4. Disorder-induced state transition of a Néel-type skyrmion. (a) The evolution of the skyrmion number N_{sk} as the increment of disorder in phase δ_P. δ_A is set to 0. The insets show the vectorial electric field textures under different values of δ_P. (b) The evolution of the skyrmion number N_{sk} as the increment of disorder in amplitude δ_A. δ_P is set to 0. The insets show the vectorial electric field textures under different values of δ_A. (c) The evolution of the skyrmion number N_{sk} when disorder in phase and amplitude coexists. (d) Demonstration of the textures of vectorial electric field with hybrid disorder.

N_{sk}, unequivocally showing a state transition from blue ($N_{sk} = 1$) to red ($N_{sk} = 0$) as disorder increases. Topological protection is confirmed by the region with bluish color, representing a minor degradation of the topological number ($N_{\mathrm{sk}} > 0.9$). We depict the four textures of the skyrmions when the hybrid disorder exists. The key features are kept when the value of δ_A is small, despite the moderate level of fluctuation in phase. The increase of δ_A can rapidly diminish the topological texture.

We attribute the robustness of the skyrmion to the unique topology in the hologram plane as shown in Figs. 1(g)–1(j). Holes or rings with near-zero values occur inside the bright spots from the amplitude distribution, driving the shape topological nontrivial. Compared with amplitude-only disorder, the phase-only disorder applied on the whole x-y plane does not break the ring and hole topology existing in the amplitude plane, leading to strong robustness as shown in Figs. 4(a)–4(b). More details can be found in the Supplemental Material [54].

We carry out similar systematic analyses for the robustness of the other five classes of skyrmions. The transition dynamics share a strong similarity with the Néel-type case, as shown in the Supplemental Material [54]. A comparison of topological protection among these quasiparticles can be found in Supplemental Material [54].

In the previous analysis, we treat the disorder in amplitude and phase as independent random variables with uniform distribution, to study the impact separately. For the

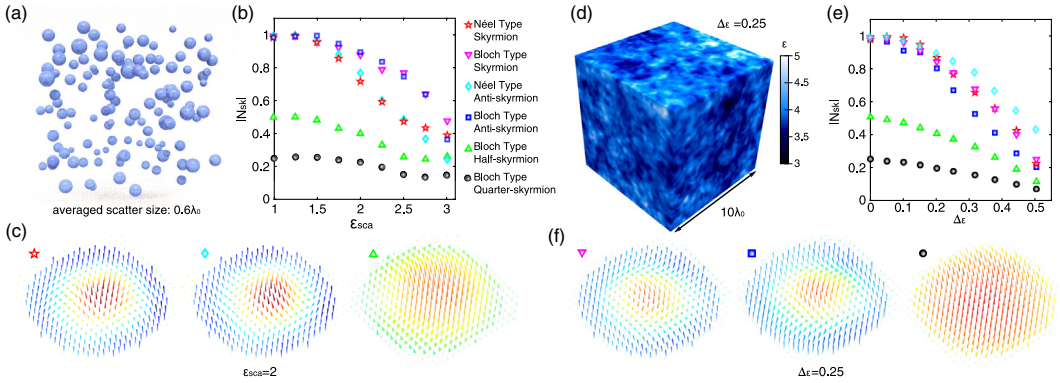

FIG. 5. The robustness of the optical skyrmions propagating through a random medium. (a) Demonstration of a discrete random medium. (b) The relationship between the absolute value of N_{sk} and the permittivity of the scatters $\varepsilon_{\mathrm{sca}}$. (c) The vectorial electric field textures when $\varepsilon_{\mathrm{sca}} = 2$. (d) Demonstration of a continuous random medium. (e) The relationship between the absolute value of N_{sk} and the standard deviation of dielectric function Δ_ε. (f) The vectorial electric field textures when $\Delta_\varepsilon = 0.25$.

sake of practical applications where the amplitude and phase are intertwined, we further investigate the randomized phase and amplitude from scattering medium. To provide a comprehensive picture, two types of random media are included, with permittivity (ε) either varying discretely [Fig. 5(a)] or continuously [Fig. 5(b)]. Correspondingly, the disorder in the medium can be controlled by the permittivity of the scatters ($\varepsilon_{\mathrm{sca}}$) in discrete random medium, or the standard deviation of the permittivity in continuous random medium (Δ_ε). By solving the Maxwell's equations numerically, we obtain the fluctuations of amplitude and phase from the realistic random medium. Similarly, the disorder of amplitude and phase can be applied to the hologram plane to test the robustness of the optical skyrmions by the evolution of the topological number N_{sk}. The results are summarized in Figs. 5(b) and 5(e), for all six types of skyrmions. Here, we use the absolute value of N_{sk}, so the antiskyrmions also have positive topological numbers. We observe a strong robustness of skyrmions against the random scattering either from homogeneous medium dispersed with scatters or medium with permittivity fluctuations. In Figs. 5(c) and 5(f), we depict the vectorial field of six skyrmions when going through medium with strong scattering ($\varepsilon_{\mathrm{sca}} = 2$ and $\Delta_\varepsilon = 0.25$). In spite of some distortion, the topological feature is unambiguously preserved. More details can be found in the Supplemental Material [54].

Discussion.—Taking full advantage of the design flexibility of vectorial holograms, we manage to numerically realize arbitrary skyrmions in real space through the topological texture of the 3D vectorial fields on a two-dimensional plane. Not limited by the six classes of skyrmions demonstrated, other quasiparticles in the skyrmions family can be achieved through our concept, such as biskyrmion, skyrmioniums, bimeron, or even quasiparticles in three dimensions [53]. The ability to produce quasiparticles in the same platform endows the possibility for a systemic comparison of the topological protection among different types of skyrmions, an important topic not covered previously in optics or in magnetics. A universal disorder-induced topological state transition is demonstrated for all six classes. More importantly, we observe an unprecedented robustness endowed by the skrymions' topology against scattering from a random medium either with scatters or continuously varying permittivity.

This discovery may shed light on both fundamental physics and practical applications, inspiring additional research in skyrmions and beyond. The robustness comparison among skyrmions with different topologies will be an interesting question in other systems in optics, magnetics, and beyond, guiding the related applications with a demand for better immunity against imperfection. Also, the robustness embedded in optical skyrmions against phase and amplitude fluctuations from a scattering medium may stimulate a new generation of photonic devices producing structured light with unique topology. The immunity against disorder in phase and amplitude ensures the skyrmion keep its topological feature after going through a random media with moderate disorder, offering new possibilities for optical communications and image.

Meanwhile, the disorder can be modeled as the imperfection on the hologram device. In this scenario, a topological hologram texture is achieved with super robustness against phase fluctuations, with a sharp contrast with the existing holograms. This may stimulate future development of topological holograms based on ultrathin metasurfaces, the latter have recently transformed the photonic design [56–62].

S. A. M. acknowledges financial support from Deutsche Forschungsgemeinschaft Cluster of Excellence e-conversion (EXC 2089111-390776260), and the Lee-Lucas Chair in Physics. H. R. acknowledges funding support from the DECRA Project (DE220101085) from the Australian Research Council. S. Z. acknowledges the financial support from Research Grants Council of Hong Kong (AoE/P-502/20, 17309021).

*changxu.liu@northumbria.ac.uk
†haoran.ren@monash.edu

[1] T. H. R. Skyrme, Nucl. Phys. **31**, 556 (1962).
[2] N. Nagaosa and Y. Tokura, Nat Nanotechnol. **8**, 899 (2013).
[3] R. Wiesendanger, Nat. Rev. Mater. **1**, 16044 (2016).
[4] A. Fert, N. Reyren, and V. Cros, Nat. Rev. Mater. **2**, 17031 (2017).
[5] A. N. Bogdanov and C. Panagopoulos, Nat. Rev. Phys. **2**, 492 (2020).
[6] Y. Tokura and N. Kanazawa, Chem. Rev. **121**, 2857 (2021).
[7] I. I. Smalyukh, Y. Lansac, N. A. Clark, and R. P. Trivedi, Nat. Mater. **9**, 139 (2010).
[8] D. Foster, C. Kind, P. J. Ackerman, J.-S. B. Tai, M. R. Dennis, and I. I. Smalyukh, Nat. Phys. **15**, 655 (2019).
[9] A. Duzgun and C. Nisoli, Phys. Rev. Lett. **126**, 047801 (2021).
[10] J. Pišljar, S. Ghosh, S. Turlapati, N. V. S. Rao, M. Škarabot, A. Mertelj, A. Petelin, A. Nych, M. Marinčič, A. Pusovnik, M. Ravnik, and I. Muševič, Phys. Rev. X **12**, 011003 (2022).
[11] I. I. Naumov, L. Bellaiche, and H. Fu, Nature (London) **432**, 737 (2004).
[12] Y. Nahas, S. Prokhorenko, L. Louis, Z. Gui, I. Kornev, and L. Bellaiche, Nat. Commun. **6**, 8542 (2015).
[13] S. Das *et al.*, Nature (London) **568**, 368 (2019).
[14] S. Das, Z. Hong, V. Stoica, M. Gonçalves, Y.-T. Shao, E. Parsonnet, E. J. Marksz, S. Saremi, M. McCarter, A. Reynoso *et al.*, Nat. Mater. **20**, 194 (2021).
[15] S. Donati, L. Dominici, G. Dagvadorj, D. Ballarini, M. De Giorgi, A. Bramati, G. Gigli, Y. G. Rubo, M. H. Szymańska, and D. Sanvitto, Proc. Natl. Acad. Sci. U.S.A. **113**, 14926 (2016).
[16] H. Ge, X.-Y. Xu, L. Liu, R. Xu, Z.-K. Lin, S.-Y. Yu, M. Bao, J.-H. Jiang, M.-H. Lu, and Y.-F. Chen, Phys. Rev. Lett. **127**, 144502 (2021).
[17] S. Tsesses, E. Ostrovsky, K. Cohen, B. Gjonaj, N. Lindner, and G. Bartal, Science **361**, 993 (2018).
[18] T. J. Davis, D. Janoschka, P. Dreher, B. Frank, F.-J. Meyer zu Heringdorf, and H. Giessen, Science **368**, eaba6415 (2020).
[19] Z.-L. Deng, T. Shi, A. Krasnok, X. Li, and A. Alù, Nat. Commun. **13**, 1 (2022).
[20] Y. Shen, Y. Hou, N. Papasimakis, and N. I. Zheludev, Nat. Commun. **12**, 1 (2021).
[21] L. Du, A. Yang, A. V. Zayats, and X. Yuan, Nat. Phys. **15**, 650 (2019).
[22] Y. Dai, Z. Zhou, A. Ghosh, R. S. Mong, A. Kubo, C.-B. Huang, and H. Petek, Nature (London) **588**, 616 (2020).
[23] X. Lei, A. Yang, P. Shi, Z. Xie, L. Du, A. V. Zayats, and X. Yuan, Phys. Rev. Lett. **127**, 237403 (2021).
[24] M. Król, H. Sigurdsson, K. Rechcińska, P. Oliwa, K. Tyszka, W. Bardyszewski, A. Opala, M. Matuszewski, P. Morawiak, R. Mazur *et al.*, Optica **8**, 255 (2021).
[25] Q. Zhang, Z. Xie, L. Du, P. Shi, and X. Yuan, Phys. Rev. Res. **3**, 023109 (2021).
[26] Y. Shen, Opt. Lett. **46**, 3737 (2021).
[27] Y. Shen, E. C. Martínez, and C. Rosales-Guzmán, ACS Photonics **9**, 296 (2022).
[28] D. Sugic, R. Droop, E. Otte, D. Ehrmanntraut, F. Nori, J. Ruostekoski, C. Denz, and M. R. Dennis, Nat. Commun. **12**, 6785 (2021).
[29] R. Gutiérrez-Cuevas and E. Pisanty, J. Opt. **23**, 024004 (2021).
[30] K. M. Song, J.-S. Jeong, B. Pan, X. Zhang, J. Xia, S. Cha, T.-E. Park, K. Kim, S. Finizio, J. Raabe *et al.*, National electronics review **3**, 148 (2020).
[31] S. Li, W. Kang, X. Zhang, T. Nie, Y. Zhou, K. L. Wang, and W. Zhao, Mater. Horiz. **8**, 854 (2021).
[32] A. J. Nederveen and Y. V. Nazarov, Phys. Rev. Lett. **82**, 406 (1999).
[33] J. Sampaio, V. Cros, S. Rohart, A. Thiaville, and A. Fert, Nat. Nanotechnol. **8**, 839 (2013).
[34] A. Sonntag, J. Hermenau, S. Krause, and R. Wiesendanger, Phys. Rev. Lett. **113**, 077202 (2014).
[35] C. Reichhardt, D. Ray, and C. J. O. Reichhardt, Phys. Rev. Lett. **114**, 217202 (2015).
[36] J. Hagemeister, N. Romming, K. Von Bergmann, E. Vedmedenko, and R. Wiesendanger, Nat. Commun. **6**, 8455 (2015).
[37] H. Oike, A. Kikkawa, N. Kanazawa, Y. Taguchi, M. Kawasaki, Y. Tokura, and F. Kagawa, Nat. Phys. **12**, 62 (2016).
[38] A. O. Leonov, Y. Togawa, T. L. Monchesky, A. N. Bogdanov, J. Kishine, Y. Kousaka, M. Miyagawa, T. Koyama, J. Akimitsu, T. Koyama, K. Harada, S. Mori, D. McGrouther, R. Lamb, M. Krajnak, S. McVitie, R. L. Stamps, and K. Inoue, Phys. Rev. Lett. **117**, 087202 (2016).
[39] S. Rohart, J. Miltat, and A. Thiaville, Phys. Rev. B **93**, 214412 (2016).
[40] J. Wild, T. N. Meier, S. Pöllath, M. Kronseder, A. Bauer, A. Chacon, M. Halder, M. Schowalter, A. Rosenauer, J. Zweck *et al.*, Sci. Adv. **3**, e1701704 (2017).
[41] D. Cortés-Ortuño, W. Wang, M. Beg, R. A. Pepper, M.-A. Bisotti, R. Carey, M. Vousden, T. Kluyver, O. Hovorka, and H. Fangohr, Sci. Rep. **7**, 4060 (2017).
[42] X. Yu, D. Morikawa, T. Yokouchi, K. Shibata, N. Kanazawa, F. Kagawa, T.-h. Arima, and Y. Tokura, Nat. Phys. **14**, 832 (2018).
[43] S.-G. Je, H.-S. Han, S. K. Kim, S. A. Montoya, W. Chao, I.-S. Hong, E. E. Fullerton, K.-S. Lee, K.-J. Lee, M.-Y. Im, and J.-I. Hong, ACS Nano **14**, 3251 (2020).
[44] K. Karube, J. S. White, V. Ukleev, C. D. Dewhurst, R. Cubitt, A. Kikkawa, Y. Tokunaga, H. M. Rønnow, Y. Tokura, and Y. Taguchi, Phys. Rev. B **102**, 064408 (2020).
[45] K. Wang, Y. Zhang, V. Bheemarasetty, S. Zhou, S.-C. Ying, and G. Xiao, Nat. Commun. **13**, 722 (2022).
[46] P. Shi, L. Du, and X. Yuan, Nanophotonics **10**, 3927 (2021).
[47] X. Li, T.-H. Lan, C.-H. Tien, and M. Gu, Nat. Commun. **3**, 998 (2012).
[48] H. Ren, W. Shao, Y. Li, F. Salim, and M. Gu, Sci. Adv. **6**, 4261 (2020).
[49] N. Mao, G. Zhang, Y. Tang, Y. Li, Z. Hu, X. Zhang, K. Li, K. Cheah, and G. Li, Proc. Natl. Acad. Sci. U.S.A. **119**, e2204418119 (2022).
[50] Y. Bao, L. Wen, Q. Chen, C.-W. Qiu, and B. Li, Sci. Adv. **7**, 0365 (2021).
[51] N. A. Rubin, A. Zaidi, A. H. Dorrah, Z. Shi, and F. Capasso, Sci. Adv. **7**, 7488 (2021).

[52] Q. Song, X. Liu, C.-W. Qiu, and P. Genevet, Appl. Phys. Rev. **9**, 011423 (2022).
[53] B. Göbel, I. Mertig, and O. A. Tretiakov, Phys. Rep. **895**, 1 (2021).
[54] See Supplemental Material at http://link.aps.org/supplemental/10.1103/PhysRevLett.129.267401 for generalized vectorial diffraction theory for the generation of arbitrary 3D vectorial fields, details of different types of skyrmions, amplitude and phase for skyrmion generation, disorder-induced phase transition for the other five classes of optical skyrmions, disorder-induced phase transition with different sets of random variables, a comparison of the topological protection for six classes of skyrmions and modeling the random medium, which includes Refs. [48,53,55].
[55] X. Zhang, Y. Zhou, K. M. Song, T.-E. Park, J. Xia, M. Ezawa, X. Liu, W. Zhao, G. Zhao, and S. Woo, J. Phys. Condens. Matter **32**, 143001 (2020).
[56] N. Yu, P. Genevet, M. A. Kats, F. Aieta, J.-P. Tetienne, F. Capasso, and Z. Gaburro, Science **334**, 333 (2011).
[57] D. Lin, P. Fan, E. Hasman, and M. L. Brongersma, Science **345**, 298 (2014).
[58] A. Arbabi, Y. Horie, M. Bagheri, and A. Faraon, Nat. Nanotechnol. **10**, 937 (2015).
[59] J. B. Mueller, N. A. Rubin, R. C. Devlin, B. Groever, and F. Capasso, Phys. Rev. Lett. **118**, 113901 (2017).
[60] R. C. Devlin, A. Ambrosio, N. A. Rubin, J. B. Mueller, and F. Capasso, Science **358**, 896 (2017).
[61] H. Ren, X. Fang, J. Jang, J. Bürger, J. Rho, and S. A. Maier, Nat. Nanotechnol. **15**, 948 (2020).
[62] M. Liu, W. Zhu, P. Huo, L. Feng, M. Song, C. Zhang, L. Chen, H. J. Lezec, Y. Lu, A. Agrawal, and T. Xu, Light Sci. Appl. **10**, 107 (2021).